Journal Pre-proof

Degradation of tetracycline antibiotic utilizing light driven-activated oxone in the presence of g-C_3N_4/ZnFe LDH binary heterojunction nanocomposite

Reza Darvishi Cheshmeh Soltani, Elham Abolhasani, Masoumeh Mashayekhi, Najla Jorfi, Grzegorz Boczkaj, Alireza Khataee

PII: S0045-6535(22)01694-0

DOI: https://doi.org/10.1016/j.chemosphere.2022.135201

Reference: CHEM 135201

To appear in: *ECSN*

Received Date: 1 April 2022

Revised Date: 17 May 2022

Accepted Date: 31 May 2022

Please cite this article as: Cheshmeh Soltani, R.D., Abolhasani, E., Mashayekhi, M., Jorfi, N., Boczkaj, G., Khataee, A., Degradation of tetracycline antibiotic utilizing light driven-activated oxone in the presence of g-C_3N_4/ZnFe LDH binary heterojunction nanocomposite, *Chemosphere* (2022), doi: https://doi.org/10.1016/j.chemosphere.2022.135201.

Author contributions

Reza Darvishi Cheshmeh Soltani: Writing-original draft, Methodology, Conceptualization. **Elham Abolhasani**: Formal analysis, Investigation. **Masoumeh Mashayekhi**: Formal analysis, Investigation. **Najla Jorfi**: Formal analysis, Investigation. **Grzegorz Boczkaj**: Writing-review & editing. **Alireza Khataee**: Writing-review & editing.

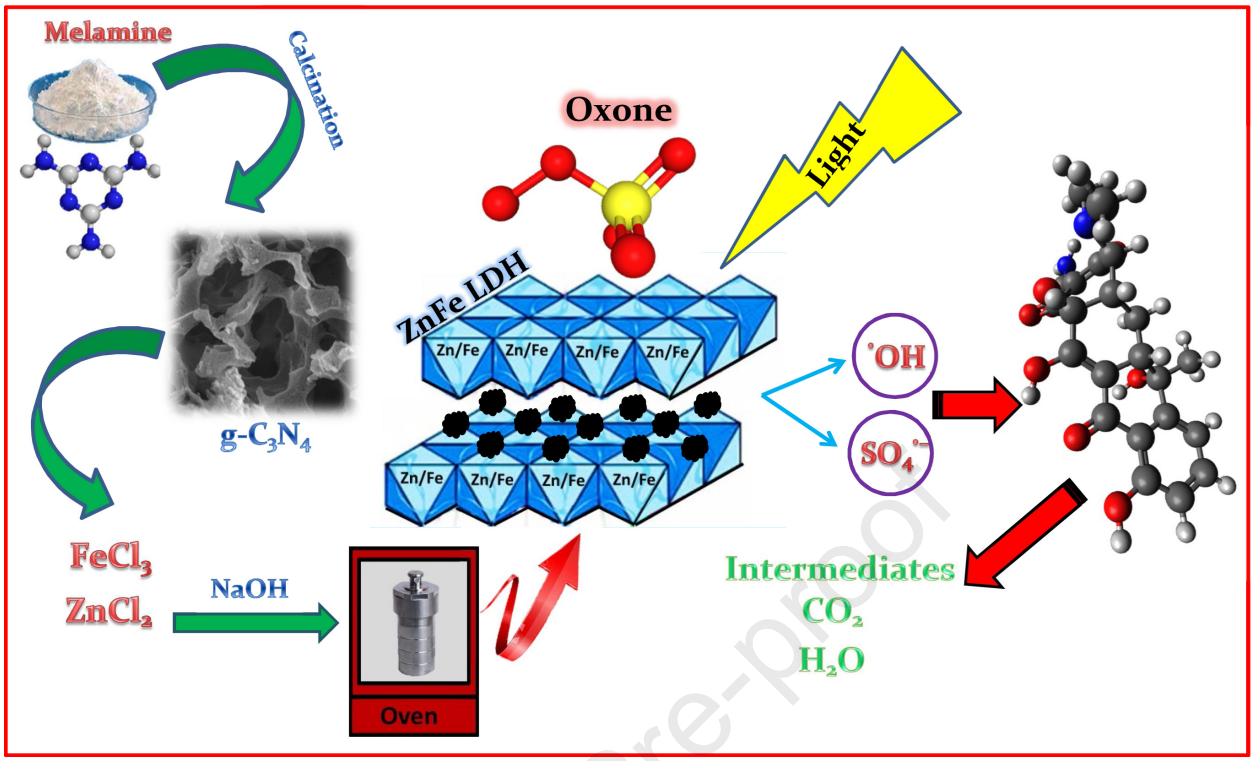

Degradation of tetracycline antibiotic utilizing light driven-activated Oxone in the presence of g-C_3N_4/ZnFe LDH binary heterojunction nanocomposite

Reza Darvishi Cheshmeh Soltani [a,*], Elham Abolhasani [a], Masoumeh Mashayekhi [a], Najla Jorfi [a], Grzegorz Boczkaj [b,c], Alireza Khataee [d,e,**]

[a]*Department of Environmental Health Engineering, School of Health, Arak University of Medical Sciences, Arak, Iran.*

[b]*Department of Sanitary Engineering, Faculty of Civil and Environmental Engineering, Gdansk University of Technology, G. Narutowicza St. 11/12, 80-233 Gdansk, Poland.*

[c]*EkoTech Center, Gdansk University of Technology, G. Narutowicza St. 11/12, 80-233 Gdansk, Poland.*

[d]*Research Laboratory of Advanced Water and Wastewater Treatment Processes, Department of Applied Chemistry, Faculty of Chemistry, University of Tabriz, 51666-16471 Tabriz, Iran*

[e]*Department of Environmental Engineering, Gebze Technical University, 41400 Gebze, Turkey*

[*] Corresponding author (communicator):

rezadarvish86@yahoo.com

[**] Corresponding author:

a_khataee@tabrizu.ac.ir

Abstract

In the present study, a binary heterojunction nanocomposite composed of graphitic carbon nitride (g-C_3N_4) and Zn/Fe-contained layered double hydroxide (ZnFe LDH) was employed as heterogeneous catalyst for the decomposition of tetracycline (TC) antibiotic utilizing Oxone and UV light irradiation. The sole use of g-C_3N_4/ZnFe LDH as adsorbent led to the negligible elimination of TC. In addition, the sole use of Oxone or UV (photolysis) and even their combination were not effective enough to degrade the target pollutant, while the combined process of g-C_3N_4/ZnFe LDH/Oxone/photolysis revealed significantly enhanced (synergistic) degradation of TC (92.4% within 30 min). Indirect detection tests for the identification of free radical species indicated the major role of both hydroxyl ($^{\bullet}OH$) and sulfate ($SO_4^{\bullet-}$) radicals in the degradation of TC by the g-C_3N_4/ZnFe LDH/Oxone/photolysis system. The elimination of TC followed a pseudo-first order kinetic model. The complete degradation of TC (degradation efficiency of 100%) was achieved within the reaction time of 25 min when ultrasound (US) was applied as enhancing agent. Furthermore, the results of total organic carbon (TOC) analysis were used to exhibit progress in the mineralization of the pollutant. The bioassay results indicated the decreased toxicity of the process effluent toward microbial population of *Escherichia coli* after the treatment.

Keywords: Tetracycline; Peroxymonosulfate; Graphitic carbon nitride; Layered double hydroxides; Heterojunction catalyst; Advanced oxidation processes (AOPs).

1. Introduction

Water contamination is proposed as one of the greatest health and environmental concerns of many developing societies (Darvishi Cheshmeh Soltani et al., 2014; Abazari et al., 2019). Due to the wide adverse effects of emerging pollutants including antibiotics, endocrine disrupting compounds, pesticides, veterinary medications and personal care products on ecosystems and human body, these compounds are nominated as target pollutants to be eliminated via various preventive and treatment strategies. Among the wide range of emerging pollutants in water, the existence of pharmaceutical compounds especially antibiotics has been considered as a global concern because of their hazards for the ecosystem and human health. The worldwide consumption of antibiotics is between 100,000 and 200,000 tons per year (Chen et al., 2019).

As a widely used antibiotic, tetracycline (TC) is commonly prescribed to treat various infections of intestines, urinary tract, skin, lymph nodes, respiratory tract and genitals because of its low price and good effectiveness (Ao et al., 2019; Chen et al., 2021b). This antibiotic compound is discharged as metabolized and unmetabolized forms into aquatic environments. As a result, it is detected and measured in the activated sludge process effluent of municipal wastewater treatment plants because of its low bio-degradability (Soltani et al., 2018). Significantly, the emergence of resistant genes and antibiotic resistant bacteria is the main problem owing to the release of antibiotic compounds into the water resources (Soltani et al., 2018; Karim and Shriwastav, 2021).

Conclusively, the degradation of TC antibiotic in water and wastewater is of great challenge considering both health and environmental aspects. Different treatment technologies have been developed and utilized for the removal of antibiotics from the aquatic phase including adsorption

process (Gao et al., 2012), electrochemical processes (Wu et al., 2012), membrane technologies (Sharma et al., 2017), conventional and advanced chemical oxidation (Anjali and Shanthakumar, 2019; Wang et al., 2019). Advanced oxidation processes (AOPs) based on the formation of free oxidizing radicals such as hydroxyl radical ($^{\bullet}OH$) and sulfate radical ($SO_4^{\bullet-}$) is attracted much more attention for the removal of antibiotics from water resources, converting the target pollutant to low-hazardous or even non-hazardous intermediates and final products (Li et al., 2022).

As sulfate radical-based chemical treatment systems, Oxone (peroxymonosulfate) activated by various agents such as light irradiation (Ao et al., 2018), ultrasonic radiation (Yin et al., 2018; Fedorov et al., 2021), heat (Ahn et al., 2021), carbonaceous materials (Shahzad et al., 2020; Soltani et al., 2020; Yang et al., 2021) and metal ions (Darvishi Cheshmeh Soltani et al., 2021; Guo et al., 2021) are extensively applied for the decomposition of emerging pollutants due to the production of free oxidizing species in the contaminated water. Graphitic carbon nitride (g-C_3N_4) with high light absorption potential, narrow band gap, high thermal stability, large surface area and simplicity of the synthesis procedure is proposed for not only photocatalytic treatment systems (Di et al., 2019; He et al., 2021b) but also for the activation of Oxone (Feng et al., 2018; Alnaggar et al., 2021).

The combination of g-C_3N_4 with other catalysts forming heterojunction is a novel method to improve the photo-induced catalytic activity due to the efficient separation of as-generated e^-/h^+ pairs (Lestari et al., 2021). As a promising and innovative technique, hydrotalcite-like structures of layered double hydroxides (LDHs) have been also used in several areas such as photocatalysis and electrochemical processes (Liu et al., 2018; Motlagh et al., 2020; He et al., 2021b). Actually, LDHs are inorganic layered materials containing divalent and trivalent metal ions, along with an n-valent anion to balance the positively charged layers (Zhao et al., 2018; Rad et al., 2022).

LDHs have attracted remarkable attention as catalyst for the advanced oxidation processes (AOPs) because of their exceptional structure. Regarding the need to synthesize and use innovative and effective heterogeneous catalysts, in the present investigation, both g-C_3N_4 and ZnFe LDH compounds were synthesized and applied as binary heterojunction nanocomposite for the synergistic activation of Oxone in the presence of UV light irradiation. Furthermore, the combination of g-C_3N_4 and ZnFe LDH could be acted as an excellent photocatalyst under UV light irradiation (Song et al., 2019).

Briefly, in the present study, batch flow-mode experimental reactors containing the binary heterojunction of g-C_3N_4/ZnFe LDH were applied to activate Oxone for the efficient removal and degradation of TC antibiotic in water. The UV light irradiation was also employed to synergistically degrade the target pollutant. Moreover, the influence of main operating parameters on the process performance was examined to assess the process capability under variable operating conditions. Finally, a bioassay was performed on the process effluent using the reference microorganism of *Escherichia coli* relying on antimicrobial effects of the undecomposed TC and its intermediates generated during the treatment process.

2. Materials and methods

2.1. Materials

Analytical grade powder of TC (molecular formula: $C_{22}H_{24}N_2O_8$; molecular weight: 444.43 g/mol) and melamine (molecular formula: $C_3H_6N_6$; molecular weight: 126.12 g/mol; purity of 99%) were obtained from Sigma-Aldrich, USA. Oxone (potassium peroxymonosulfate) with molecular weight of 152.2 g/mol was supplied from Merck, Germany. Other reagents and

chemicals such as $FeCl_3.6H_2O$, $ZnCl_2$, NaOH, C_2H_5OH (EtOH), CH_3OH (MeOH), $C_4H_{10}O$ (tert-Butyl alcohol, TBA) and HCl were also obtained from Merck, Germany.

2.2. Preparation of heterojunction nanocomposite

For the synthesis of g-C_3N_4/ZnFe LDH heterojunction nanocomposite, firstly, 2 g melamine was added to 50 mL distilled water and then heated on a hot plate at 60°C under gentle mechanical stirring. The resulting sample was dried in an oven at 80°C. Finally, it was calcined in an electric furnace for 2 h at 550°C to attain g-C_3N_4 sample. In the next step, as-synthesized g-C_3N_4 nanostructures (weight percent of 0.5%), together with 2 mM $FeCl_3.6H_2O$ and 6 mM $ZnCl_2$, were dissolved in 100 mL distilled water. Then it was homogenized using mechanical stirrer for 20 min. Afterwards, 1 N sodium hydroxide was gradually added to the above solution under mechanical stirring and argon gas at 60°C until pH reached around 9.0. The resulting precipitate was poured into a hydrothermal vessel and heated in an oven at 120 °C for 24 h. After that, the sample was washed several times on the filter using distilled water and ethanol to reach neutral pH of 7.0. Ultimately, the obtained g-C_3N_4/ZnFe LDH heterojunction nanocomposite was dried in an oven at 90°C until reaching a constant weight. It was stored in a desiccator until use.

2.3. Experimental protocols

Batch flow-mode reactors were used to remove TC antibiotic from water samples. One 6-W UVC lamp was utilized to irradiate the reactor containing TH (photolysis process). An Elma ultrasonic bath made by Italy with an input power of 320 W and working frequency of 80 kHz was applied to enhance the process effectiveness using ultrasound (US). Firstly, the role of adsorption of TC onto g-C_3N_4, ZnFe LDH and g-C_3N_4/ZnFe LDH nanocomposite in the removal of TC was investigated. Then, the efficiency of different processes involved in the removal of

TC was determined under the same operating conditions. One-factor-at-a-time statistical approach was applied for the experimental design due to its simplicity. According to the results, the most efficient process for the decomposition and removal of the pollutant was selected for conducting the rest of experiments. Oxidizing agents involved in the decomposition of TC pollutant were indirectly identified using TBA and EtOH alcohols. The effect of important operating variables such as initial pH (natural, neutral and basic pH), the amount of g-C_3N_4/ZnFe LDH nanocomposite (0.05−0.3 g/L), the pollutant concentration (10−55 μM) and the Oxone concentration (0.1−0.5 mM) on the reactor performance in terms of TC removal was examined. Finally, bio-toxicity test was performed on the process effluent under selective operating conditions.

2.4. Analysis of TC and characterization

To determine the efficiency of the treatment process, the residual concentration of TC in the process effluent was measured using high-performance liquid chromatography (HPLC) technique utilizing UV detector of 360 nm wavelength. A mixture of methanol, oxalic acid and acetonitrile was prepared as mobile phase of the HPLC device. In this regard, 2-ml samples were withdrawn from the batch flow-mode reactor at regular time intervals based on the experimental design. They were centrifuged and filtered before the HPLC analysis. Progress in the mineralization of TC was checked by the total organic carbon (TOC) analyzer (Skalar, the Netherlands). Scanning electron microscopy (SEM) and energy dispersive X-ray (EDX) spectroscopy were performed to exhibit morphological characteristics of the samples (TESCAN microscope, model: Mira3, Czech Republic). In addition, elemental mapping was carried out to show elemental distribution of the synthesized compounds. Fourier transform infrared (FTIR) spectroscopy (Bruker Co., Germany) was used to identify surface functional groups and crystal

structure of the samples via a non-destructive route. X-ray diffraction analysis (XRD) was utilized to specify the crystallographic composition of the samples (Tongda, model: TD-3700, China). Differential reflectance spectroscopy (DRS) analysis (S250, Analytik Jena Co., Germany) using wavelength range of 400–1000 nm was employed to study the spectral properties of the solid samples on the basis of not only surface reflected light but also internally reflected light. Moreover, band gap energy of the synthesized catalysts could be determined via the DRS analysis. Contribution of the adsorption process to the elimination of TC was determined via the adsorption equation (Soltani et al., 2015; Durrani et al., 2022). Bio-toxicity of the process effluent containing undecomposed TC molecule and its byproducts was examined using plate count method using *Escherichia coli (E. coli)* as the reference microorganism. Briefly, 0.1 mL microbial suspension along with 0.5 mL effluent sample was dispersed on the agar plate surface. The plate was incubated at 37ºC for 24 h. The abovementioned procedure was used for the treated and untreated samples under the same conditions.

3. Results and discussion

3.1. Characterization (SEM-EDX-Map, XRD, FTIR, DRS)

Surface structure of the samples was examined by conducting SEM analysis. The SEM images and corresponding EDX-mapping graphs are represented in Fig. 1. Fig. 1a shows surface structure of the g-C_3N_4 containing nanostructures with irregular shapes and high porosity. This construction gives a good potential to enhance the catalytic conversion of TC via increasing reaction sites. The EDX analysis was performed as a rapid, efficient and precise technique to specify elemental composition of the sample using electron microscope through a non-destructive approach. The corresponding EDX micrograph of the g-C_3N_4 exhibits the existence

of C and N elements in the composition (Fig. 1b). Using SEM and EDX, elemental mapping of the g-C_3N_4 on the basis of gathering highly particular elemental composition details upon specific area of the sample represents uniform distribution of the elements in the g-C_3N_4 structure. An example of SEM images of the ZnFe LDH is shown in Fig. 1c. As displayed, nanostructures of the ZnFe LDH are well-distributed in the sample promoting reactivity of the catalyst to generate more oxidizing species in the solution due to the fine size and consequently large surface area. Based on the EDX micrograph (Fig. 1d), the ZnFe LDH is mainly composed of Zn and Fe with specified peaks in the graph. The distribution of as-mentioned elements is exhibited via an elemental mapping placed on the graph. The surface structure of as-synthesized binary heterojunction of g-C_3N_4/ZnFe LDH is displayed via Fig. 1e. As can be seen, after the combination of g-C_3N_4 with ZnFe LDH, the g-C_3N_4 nanostructures are covered on the ZnFe LDH composite, revealing circular particles with some cracks on the surface. As shown in the EDX micrograph (Fig. 1f), this binary heterojunction is comprised of C, N, Zn and Fe elements which can be found in the structure of composing components. Distribution of the elements is also depicted.

XRD patterns of the samples are illustrated in Fig. 2a. The g-C_3N_4 pattern shows two representative peaks placed at 12.7 and 27.8° corresponding to (100) and (002) planes of the crystalline structure, indicating the stacking of conjugated aromatic compounds in the interlayers and constructional pattern of the composition, respectively (Zeng et al., 2020; Lestari et al., 2021; Yu et al., 2021). The first peak had lower intensity than the later peak, exhibiting insignificant stacking of conjugated aromatic compounds in the interlayers of the binary heterojunction due to the calcination. In the case of ZnFe LDH, the peaks placed at 31.9, 34.5, 36.4, 47.5, 56.7 and 62.8 corresponding to (101), (009), (015), (012), (110) and (113) planes

198 were the routine LDH characteristic peaks, respectively (Wang et al., 2020). The binary
199 heterojunction pattern exhibits the presence of both LDH and g-C_3N_4 characteristic peaks with
200 lower intensity of the LDH peaks compared with that of g-C_3N_4 because of the lower amounts of
201 LDH in the binary heterojunction.

202 Surface functional groups of the samples were determined through the FTIR analysis (Fig. 2b).
203 Accordingly, FTIR spectrum of the g-C_3N_4 exhibits the stretching vibration peak of N–H bond
204 centered at wavenumber of 3200 cm^{-1} (Di et al., 2019; Lestari et al., 2021). The peaks in the
205 wavenumber range of 1250–1470 cm^{-1} and 1480–1660 cm^{-1} can be attributed to the stretching
206 oscillation of C=N and C–N bonds, respectively (Di et al., 2019). The vibrating peak located at
207 813 cm^{-1} is associated with s-triazine rings of the g-C_3N_4 (Yu et al., 2021). FTIR spectrum of the
208 ZnFe LDH sample reveals a sharp peak centered at wavenumber of 3450 cm^{-1} as a result of the
209 existence of O–H stretching bond of the interlayer water molecules and layered hydroxyl groups
210 of the sample (Qin et al., 2019). In addition, the sharp peak placed around 600 cm^{-1} is related to
211 the stretching vibration of M–O or M–OH bonds (M describes Fe and Zn) (Di et al., 2019;
212 Naderi and Darvishi Cheshmeh Soltani, 2021). As can be clearly seen in Fig. 2b, FTIR spectrum
213 of the binary heterojunction of g-C_3N_4/ZnFe LDH nanocomposite is similar to the pure g-C_3N_4.
214 This indicated no influence of the ZnFe LDH on the chemical structure of the g-C_3N_4. On the
215 other hand, the structure of g-C_3N_4 in the binary heterojunction nanocomposite was not
216 destroyed during the fabrication process.

217 The DRS spectroscopy with the wavelength ranging from 200 to 800 nm was utilized to examine
218 optical characteristics of the fabricated samples (Fig. 3). In the case of g-C_3N_4, as displayed in
219 Fig. 3a, four distinct absorption peaks in the UV wavelength region (225, 265, 290 and 340 nm)
220 were observed exhibiting its UV-light absorption properties. The ZnFe LDH compound shows

four main absorption peaks where the two were appeared in the UV light wavelength region (230 and 395 nm) assigning to the charge transfer of metal-ligand in the layered compound, and the other two absorption peaks located in the visible light region wavelength range (485 and 570 nm) are attributed to metal ions transitions in the layered structure (Fig. 3b). In the UV light wavelength region, the optical absorption peaks of ZnFe LDH and g-C_3N_4 were also observed in the case of the heterojunction nanocomposite of g-C_3N_4/ZnFe LDH (Fig. 3c), thereby indicating the presence of ZnFe LDH and g-C_3N_4 in the nanocomposite structure (Jo and Tonda, 2019). Furthermore, overlapping the absorption peaks intimated the effective interaction between the components in the structure of g-C_3N_4/ZnFe LDH heterojunction. The enhanced optical absorption in the UV light wavelength range makes the heterojunction nanocomposite an efficient catalyst under UV light irradiation. According to the obtained DRS spectra, the band gap energy (E_g) of the samples was calculated based on absorption coefficient (α) and frequency of light radiation (ν) as displayed in the following formula:

$$\alpha h\nu = A\left(h\nu - E_g\right)^{\frac{n}{2}} \quad (1)$$

where h and n are the Planck's constant and optical absorption index, respectively. For the calculation of E_g, $(\alpha h\nu)^2$ was plotted versus $h\nu$ as exhibited in Fig. 3a, b and c. Accordingly, E_g values obtained for g-C_3N_4, ZnFe LDH and g-C_3N_4/ZnFe LDH nanocomposite were 3.14, 3.76 and 2.98 eV, respectively. The results indicated reduction in the band gap energy of the g-C_3N_4/ZnFe LDH heterojunction nanocomposite in comparison with the individual compounds of g-C_3N_4 and ZnFe LDH. The decreased band gap energy of the heterojunction nanocomposite resulted in the intensified catalytic decomposition of TC due to the reduced recombination rate of e^-/h^+ pairs generated in the catalytic system (Kim and Kan, 2016).

3.2. Comparative study results

Preliminary experiments were performed to specify the role of individual processes in the removal of TC antibiotic. In this regard, the adsorption process usually play unavoidable role during elimination of the target pollutant using heterogeneous catalysts. Thus, the treatment process was conducted in the presence of g-C_3N_4, ZnFe LDH and g-C_3N_4/ZnFe LDH under dark condition without the addition of Oxone to determine the adsorption potential of the synthesized binary heterojunction nanocomposite and its components. The results of this set of experiments are shown in Fig. S1. Using g-C_3N_4, ZnFe LDH and g-C_3N_4/ZnFe LDH compounds, the adsorption efficiencies of 8.0, 8.8 and 9.2% were obtained. Accordingly, the Langmuir model was applied to predict maximum adsorption capacity of the samples (Soltani et al., 2009; Darvishi Cheshmeh Soltani et al., 2011):

$$\frac{C_e}{q_e} = \frac{1}{kq_m} + \frac{1}{q_m} C_e \qquad (2)$$

where q_m (µM/g) expresses the maximum capacity of the adsorbent to adsorb TC molecules, while q_e (µM/g) represents the capacity of adsorption at specific equilibrium time. The constant K defines the affinity of solid adsorbent for the TC molecules (L/µM). Based on the Langmuir-based isotherm modeling, the q_m values of 0.36, 0.50 and 0.65 µM/g were obtained when g-C_3N_4, ZnFe LDH and g-C_3N_4/ZnFe LDH compounds were used as adsorbents, respectively. The results indicated insignificant contribution of the adsorption process to the removal of TC. In the following, Oxone alone, photolysis using UV lamp alone and the combined process of Oxone/photolysis were utilized for the removal of TC without the heterogeneous catalyst. The application of Oxone, photolysis and Oxone/photolysis resulted in the degradation efficiency of 5.6, 9.2 and 42.0%, respectively (Fig. 4a). Obviously, the sole use of Oxone and photolysis led to

the negligible degradation of TC, while their combination resulted in the notable efficiency of 42.0%. This can be explained by the fact that UV irradiation activates Oxone to generate free oxidizing radicals in the reactor:

$$HSO_5^- + h\nu \rightarrow SO_4^{\bullet -} + OH^- \quad (3)$$

As shown in Fig. 4a, the utilization of g-C_3N_4/Oxone (23.6%) and g-C_3N_4/photolysis (32.8%) led to the enhanced degradation of TC in comparison with the sole use of Oxone (5.6%) or photolysis (9.2%). For the g-C_3N_4/Oxone process, no remarkable degradation efficiency of TC was attained when g-C_3N_4 alone was applied for the activation of Oxone, suggesting low reactivity of g-C_3N_4 toward the Oxone to generate radical species (Feng et al., 2018). In agreement with our results, Chen et al. (2021) reported an insignificant degradation efficiency of 9.4% in the g-C_3N_4/Oxone treatment system for the removal of 4-chlorophenol (Chen et al., 2021a). For the g-C_3N_4/photolysis, the catalytic properties of the synthesized g-C_3N_4 arise from its narrow band gap energy and consequently high photo-sensitivity (Gholami et al., 2020). The binary heterojunction nanocomposite of g-C_3N_4/ZnFe LDH was employed to perform the rest of experiments. Using g-C_3N_4/ZnFe LDH/Oxone and g-C_3N_4/ZnFe LDH/photolysis processes, the degradation efficiencies of 57.2 and 68.4% were attained, respectively, which indicated the major contribution of ZnFe LDH to the degradation of TC. In a similar study, Zhao et al. (2018) utilized both Fe-Co LDH/Oxone and $CoMn_2O_4$/Oxone treatment systems for the degradation of an organic dye. They reported a degradation efficiency of 60% within short reaction time which was associated with high Oxone activation potential of the layered compounds and rapid generation rate of the sulfate radical (Zhao et al., 2018). In the case of ZnFe LDH, high activation potential and superior chemical stability is ascribed to the valence changes between Zn and Fe ions (Zhao et al., 2018).

Similarly, a bimetallic LDH catalyst containing Co and Mn was successfully used by He et al. (2021) for the degradation of nitroimidazoles through the activation of Oxone. Based on their analysis and interpretation, the alteration of bimetallic valence in Co-Mn LDH structure donated electron for the activation of Oxone (He et al., 2021a). The presence of Fe ions in the structure of ZnFe LDH improves the generation of free oxidizing radicals (Soltani et al., 2018; Guo et al., 2021):

$$Fe(III) + HSO_5^- \rightarrow Fe(II) + SO_5^{\bullet -} + H^+ \quad (4)$$

$$Fe(II) + HSO_5^- \rightarrow SO_4^{\bullet -} + Fe(III) + OH^- \quad (5)$$

In addition, it is demonstrated that the combination of g-C_3N_4 and layered double hydroxide compounds such as ZnFe LDH enhances water treatment efficiency in comparison with that of LDH alone or pure g-C_3N_4 due to the reduced e^-/h^+ recombination rate (Jo and Tonda, 2019; Song et al., 2019). Furthermore, as can be observed in Fig. 4a, the efficiency of 92.4% was obtained when the g-C_3N_4/ZnFe LDH/Oxone/photolysis process was used for the decomposition of TC. In this regard, the binary heterojucntion nanocomposite is not only played the heterogeneous activator role for Oxone to form radical species but also acted as the heterogeneous photocatalyst for UV light irradiation. Under UV light irradiation, the e^-/h^+ pairs of the binary g-C_3N_4/ZnFe LDH heterojucntion were produced due to the stimulation of both g-C_3N_4 and ZnFe LDH (Song et al., 2019; Zeng et al., 2020):

$$\text{g} - C_3\text{N}_4/\text{ZnFe LDH} + \text{h}\nu \rightarrow h^+ + e^- \quad (6)$$

Meanwhile, the generated electrons react with Oxone to form both $^{\bullet}OH$ and $SO_4^{\bullet -}$ radicals:

$$HSO_5^- + e^- \rightarrow SO_4^{\bullet -} + OH^- \quad (7)$$

$$SO_4^{\bullet -} + OH^- \rightarrow SO_4^{2-} + {}^{\bullet}OH \quad (8)$$

Because of the asymmetrical structure of Oxone and the conversion of sulfate to hydroxyl radicals, simultaneous formation of such radicals is feasible (Feng et al., 2018). Jin and coworkers used g-C_3N_4 in combination with Co_3O_4 for the activation of Oxone to degrade TC. Based on their results, a degradation efficiency of 99% was obtained under visible light irradiation of Xenon lamp (Jin et al., 2020). Ultimately, the synergy percent was calculated considering the application of g-C_3N_4/ZnFe LDH/Oxone, g-C_3N_4/ZnFe LDH/photolysis and g-C_3N_4/ZnFe LDH/Oxone/photolysis processes by the following equation:

$$Synergy\ (\%) = \frac{k_{g-C_3N_4/ZnFe\ LDH/Oxone/Photolysis} - (k_{g-C_3N_4/ZnFe\ LDH/Oxone} + k_{g-C_3N_4/ZnFe\ LDH/Photolysis})}{k_{g-C_3N_4/ZnFe\ LDH/Oxone/Photolysis}} \quad (9)$$

According to the obtained reaction rate constants (Fig. 4b), the synergy percent of 18.9% was calculated using the above formula, indicating the significant increase in the degradation rate of TC when both Oxone and photolysis were simultaneously utilized in the presence of g-C_3N_4/ZnFe LDH. Progress in the mineralization of the target compound was also checked within the reaction time of 30 min based on the results of TOC analysis. As a result, the mineralization efficiency of 33.5% was obtained within the short reaction time of 30 min.

3.3. Enhancing techniques

To further enhance efficiency of the g-C_3N_4/ZnFe LDH/Oxone/photolysis process in the removal of TC, hydrogen peroxide (H_2O_2) and ultrasound (US) were implemented as chemical and physical enhancing agents, respectively. The results are provided in Fig. 5a. Using H_2O_2, the degradation efficiency of TC increased from 92.4 to 100% within the reaction time of 30 min.

330 The addition of hydrogen peroxide improves the formation of $^{\bullet}OH$ radicals in the reactor as
331 represented in the following equation:

332 $$H_2O_2 + e^- \rightarrow {}^{\bullet}OH + OH^- \quad (10)$$

333 The addition of H_2O_2 in the presence of ZnFe LDH is considerably reactive for the degradation
334 of pollutants through the interaction with Fe ions (Feng et al., 2018). The complete degradation
335 of TC was achieved within the reaction time of 25 min when US was applied as enhancing agent.
336 The US alone is used for the degradation of various pollutants as well as its integration with
337 other treatment processes (Gągol et al., 2019; Fedorov et al., 2022). Actually, the formation of
338 $^{\bullet}OH$ is expected under ultrasonic irradiation as a result of the water dissociation (Soltani et al.,
339 2019). In the meantime, Oxone can be further activated under ultrasonic irradiation:

340 $$HSO_5^- + US \rightarrow SO_4^{\bullet -} + {}^{\bullet}OH \quad (11)$$

341 The US creates microcirculation zones in the fluid causing formation, growth and collapse of
342 cavitation bubbles ("hot spot" phenomenon) around the solid heterojunction nanocomposite
343 because of lower tensile strength toward the solid-liquid intersection, leading to the intensified
344 water dissociation and "sonoluminescence" phenomenon. During the "sonoluminescence"
345 phenomenon, light is emitted as a result of cavitation bubbles collapse with extremely high
346 temperature and pressure, thereby exciting the heterojunction catalyst of g-C_3N_4/ZnFe LDH to
347 generate more e^-/h^+ pairs (Gholami et al., 2020). The US-induced e^-/h^+ pairs were significantly
348 segregated by the binary heterojunction nanocomposite as depicted in the following equation (He
349 et al., 2020):

350 $$\text{g} - C_3\text{N}_4/\text{ZnFe LDH} + \text{US} \rightarrow \text{g} - C_3\text{N}_4(h^+ + e^-) + \text{ZnFe LDH}\ (h^+ + e^-) \quad (12)$$

Consequently, the implementation of US led to more enhancing effect on effectiveness of the g-C_3N_4/ZnFe LDH/Oxone/photolysis process than that of H_2O_2.

3.4. Antioxidant effect

Alcoholic compounds of TBA and EtOH were added to the g-C_3N_4/ZnFe LDH/Oxone/photolysis process in order to indirectly specify the contribution of free oxidizing radicals to the degradation of TC. The experiments were performed under the same operational parameters. For this purpose, the degradation efficiencies of TC and corresponding reaction rate constants (k_{obs}) were determined in the presence of TBA and EtOH in comparison with the scavenger-free treatment reactor. TBA is recognized as potential $^{\bullet}OH$ scavenger (6.0×10^8 M^{-1} s^{-1}), which is higher than its $SO_4^{\bullet-}$ scavenging potential (4.0×10^5 M^{-1} s^{-1}) (Fedorov et al., 2020). Nevertheless, EtOH can scavenge both $^{\bullet}OH$ ($1.2\text{-}2.8\times10^9$ M^{-1} s^{-1}) and $SO_4^{\bullet-}$ ($1.6\text{-}7.7\times10^7$ M^{-1} s^{-1}), thus it can be used to quench both $^{\bullet}OH$ and $SO_4^{\bullet-}$ radicals (Xie et al., 2019). In the presence of TBA and EtOH, the degradation efficiency of TC decreased from 92.4% (k_{obs}: 0.0847 min^{-1}) to 80.4% (k_{obs}: 0.0543 min^{-1}) and 52.4% (k_{obs}: 0.0261 min^{-1}), respectively (Fig. 5a and b). Based on these data, the following equations were used to prove the role of $^{\bullet}OH$ and $SO_4^{\bullet-}$ radicals in the degradation of TC antibiotic:

$$Role\ of\ {}^{\bullet}OH = \frac{k_{obs}-k_{obs,TBA}}{k_{obs}} \times 100 \quad (13)$$

$$Role\ of\ SO_4^{\bullet-} = \frac{k_{obs,TBA}-k_{obs,EtOH}}{k_{obs}} \times 100 \quad (14)$$

Based on the above equations, the role of $^{\bullet}OH$ in the degradation of TC was 36.0%, while the role of $SO_4^{\bullet-}$ was 33.3%. This indicated that $^{\bullet}OH$ played a little more notable role than $SO_4^{\bullet-}$ in the decomposition of TC by the g-C_3N_4/ZnFe LDH/Oxone/photolysis process. In agreement with

372 our results, Ramachandran et al. (2021) confirmed the major role of both $SO_4^{\bullet-}$ and $^{\bullet}OH$ radicals
373 in the degradation of organic dye utilizing NiCo-LDH/Oxone process (Ramachandran et al.,
374 2021).

375 *3.5. Effect of operating parameters*

376 The main operating parameters of solution pH, TC concentration, catalyst dosage and Oxone
377 concentration were selected to assess effectiveness of the g-C_3N_4/ZnFe LDH/Oxone/photolysis
378 process under variable operating conditions and to determine the optimum conditions for the
379 operation of the treatment process (Fig. 6). Three distinct initial pHs of 4.5 (natural pH), 7.0
380 (neutral pH) and 9.0 (basic pH) were selected to determine the influence of solution pH on the
381 reactor performance. At pH values of 4.5, 7.0 and 9.0, the degradation efficiencies of TC were
382 92.4, 95.2 and 98.8%, respectively (Fig. 6a). Thus, the degradation of TC slightly increased with
383 increasing the initial pH. Acidic pH causes disintegration of the generated free oxidizing radicals
384 resulting in the reduced process performance. The enhanced efficiency of the process at basic pH
385 could be related to the presence of more hydroxyl ions (OH^-) on the heterojucntion
386 nanocomposite surface which can get further oxidized to hydroxyl radicals (Karim and
387 Shriwastav, 2021). Moreover, in the presence of OH^- ions, sulfate radicals are converted to
388 hydroxyl radicals with higher oxidizing potential (Cai et al., 2015; Xie et al., 2019). Under basic
389 conditions, the intense affinity between the heterojucntion nanocomposite and negatively
390 charged TC molecules may improve the degradation efficiency of TC. Furthermore, the TC
391 molecule with rich electrical density on its ring system is prone to attract $^{\bullet}OH$ radicals, resulting
392 in the enhanced elimination of TC in basic conditions (Jo and Tonda, 2019). However, it should
393 be noted that excessive OH^- ions accumulated on the nanocomposite surface react with as-
394 generated holes, reducing degradation of the target pollutant.

Increasing the dosage of g-C_3N_4/ZnFe LDH from 0.05 to 0.2 g/L led to increasing the degradation of TC from 74.4 to 92.4%, respectively (Fig. 6b). However, its increase to 0.3 g/L resulted in a slight decrease in the degradation efficiency (86.8%). Increasing the amount of g-C_3N_4/ZnFe LDH improves surface reactive sites forming more radical species such as $^{\bullet}OH$ and $SO_4^{\bullet-}$ to accelerate the degradation of TC antibiotic. Nevertheless, excessive amount of the nanocomposite catalyst may scavenge the generated radical species by metallic Zn or Fe sites, thereby reducing the radical species accessible for the decomposition of TC (Feng et al., 2018; Hong et al., 2020). Moreover, higher amounts of catalyst increase turbidity of the bulk solution leading to lower effectiveness of UV absorption by the heterojunction nanocomposite (Fernandes et al., 2020). The effect of solute (TC) concentration on its degradation was explored in the range of 10-55 µM (Fig. 6c). Clearly, the efficiency increased from 60.0 to 92.4% with decreasing the initial concentration of TC from 55 to 25 µM, respectively. At initial concentrations of 15 and 10 µM, the complete degradation of TC was achieved in 30 and 25 min, respectively. The increased process efficiency with decreasing TC concentration could be attributed to the reasons as follows (Dou et al., 2020): 1) The number of oxidizing species is constant in the reactor; thus, increasing TC concentration leads to the increased competition between limited oxidizing species to react with the target pollutant. 2) The transmittance of the bulk solution will be adversely influenced when the solute concentration increases. This results in the diminished adsorption of emitted photons by the heterojucntion nanocomposite, thereby reducing the number of radical species in the reactor. 3) As-generated intermediate byproducts compete with the parent compound for interaction with radical species when the initial concentration of TC increases, declining the process efficiency.

417 The process efficiency increased with the addition of higher amounts of Oxone (Fig. 6d).
418 Increasing Oxone from 0.1 to 0.5 mM improved the efficiency from 70.0 to 95.6%, respectively.
419 As can be seen, the increase in the Oxone concentration from 0.4 to 0.5 mM caused negligible
420 increase (about 3.0%) in the efficiency. Addition of optimized concentration of Oxone, as the
421 source of oxidizing radicals, results in the formation of appropriate amounts of radical species
422 such as $^{\bullet}OH$ and $SO_4^{\bullet-}$ to efficiently decompose TC. At high concentration of Oxone, as-
423 generated $SO_4^{\bullet-}$ radicals interacts with itself generating weaker oxidizing agent of persulfate. In
424 addition, it might be destroyed by excess Oxone molecules creating $SO_5^{\bullet-}$ radical with lower
425 oxidation potential; thus, unfavorably influencing the decomposition efficiency of TC (Hong et
426 al., 2020). The results of bio-toxicity assessment on effluent of the g-C_3N_4/ZnFe
427 LDH/Oxone/photolysis process showed the improved growth of gram-negative bacilli of *E. coli*
428 (2000 CFU/100 mL) during the incubation in comparison with the untreated water sample (400
429 CFU/100 mL). This pointed out the decrease in the bio-toxicity of the TC-contained water
430 sample after the treatment process.

431 **4. Conclusions**

432 In this investigation, the binary heterojunction nanocomposite of g-C_3N_4/ZnFe LDH was
433 fabricated and successfully applied for the catalytic decomposition of tetracycline antibiotic in
434 the presence of Oxone and UV light irradiation. SEM-EDX, XRD and FTIR results revealed the
435 synthesis of g-C_3N_4/ZnFe LDH with suitable structure for the catalytic conversion of the target
436 pollutant. The role of both hydroxyl and sulfate radicals in the degradation of the pollutant was
437 indirectly verified using scavenging compounds. The treatment process effectiveness was
438 enhanced using hydrogen peroxide and ultrasonic irradiation. Increasing the Oxone
439 concentration and initial pH, along with decreasing the pollutant concentration, favored the

process efficiency. Operation of the process under natural pH conditions improves cost-efficiency of the process due to the lack of need to add chemical agents for pH adjustment. Based on the results, optimization of the dosage of the binary heterojunction nanocomposite is essential for the process operation. The growth of more colonies of *E. coli* indicated lower bio-toxicity of the treated water sample than that of untreated sample. Conclusively, the treatment process of g-C_3N_4/ZnFe LDH/Oxone/photolysis can be effectively utilized for the remediation of aquatic environments contaminated by antibiotic compounds.

Acknowledgements

The authors acknowledge Arak University of Medical Sciences (Iran) for all supports provided.

References

Abazari, R., Mahjoub, A.R., Sanati, S., Rezvani, Z., Hou, Z., Dai, H., 2019. Ni–Ti layered double hydroxide@ graphitic carbon nitride nanosheet: a novel nanocomposite with high and ultrafast sonophotocatalytic performance for degradation of antibiotics. Inorganic Chemistry 58, 1834-1849.

Ahn, Y.-Y., Choi, J., Kim, M., Kim, M.S., Lee, D., Bang, W.H., Yun, E.-T., Lee, H., Lee, J.-H., Lee, C., 2021. Chloride-Mediated enhancement in Heat-Induced activation of peroxymonosulfate: New reaction pathways for oxidizing radical production. Environmental Science & Technology 55, 5382-5392.

Alnaggar, G., Hezam, A., Drmosh, Q., Ananda, S., 2021. Sunlight-driven activation of peroxymonosulfate by microwave synthesized ternary MoO_3/Bi_2O_3/g-C_3N_4 heterostructures for boosting tetracycline hydrochloride degradation. Chemosphere 272, 129807.

461 Anjali, R., Shanthakumar, S., 2019. Insights on the current status of occurrence and removal of
462 antibiotics in wastewater by advanced oxidation processes. Journal of Environmental
463 Management 246, 51-62.
464 Ao, X., Liu, W., Sun, W., Cai, M., Ye, Z., Yang, C., Lu, Z., Li, C., 2018. Medium pressure UV-
465 activated peroxymonosulfate for ciprofloxacin degradation: Kinetics, mechanism, and
466 genotoxicity. Chemical Engineering Journal 345, 87-97.
467 Ao, X., Sun, W., Li, S., Yang, C., Li, C., Lu, Z., 2019. Degradation of tetracycline by medium
468 pressure UV-activated peroxymonosulfate process: influencing factors, degradation pathways,
469 and toxicity evaluation. Chemical Engineering Journal 361, 1053-1062.
470 Cai, C., Zhang, H., Zhong, X., Hou, L., 2015. Ultrasound enhanced heterogeneous activation of
471 peroxymonosulfate by a bimetallic Fe–Co/SBA-15 catalyst for the degradation of Orange II in
472 water. Journal of Hazardous Materials 283, 70-79.
473 Chen, L., Xing, K., Shentu, Q., Huang, Y., Lv, W., Yao, Y., 2021a. Well-dispersed iron and
474 nitrogen co-doped hollow carbon microsphere anchoring by g-C_3N_4 for efficient
475 peroxymonosulfate activation. Chemosphere 280, 130911.
476 Chen, M., Wu, P., Huang, Z., Liu, J., Li, Y., Zhu, N., Dang, Z., Bi, Y., 2019. Environmental
477 application of MgMn-layered double oxide for simultaneous efficient removal of tetracycline
478 and Cd pollution: Performance and mechanism. Journal of Environmental Management 246,
479 164-173.
480 Chen, X., Zhou, J., Chen, Y., Zhou, Y., Ding, L., Liang, H., Li, X., 2021b. Degradation of
481 tetracycline hydrochloride by coupling of photocatalysis and peroxymonosulfate oxidation
482 processes using CuO-$BiVO_4$ heterogeneous catalyst. Process Safety and Environmental
483 Protection 145, 364-377.

Darvishi Cheshmeh Soltani, R., Naderi, M., Boczkaj, G., Jorfi, S., Khataee, A., 2021. Hybrid metal and non-metal activation of Oxone by magnetite nanostructures co-immobilized with nano-carbon black to degrade tetracycline: Fenton and electrochemical enhancement with bio-assay. Separation and Purification Technology 274, 119055.

Darvishi Cheshmeh Soltani, R., Rezaee, A., Khataee, A., Godini, H., 2014. Optimisation of the operational parameters during a biological nitrification process using response surface methodology. The Canadian Journal of Chemical Engineering 92, 13-22.

Darvishi Cheshmeh Soltani, R., Rezaee, A., Shams Khorramabadi, G., Yaghmaeian, K., 2011. Optimization of lead (II) biosorption in an aqueous solution using chemically modified aerobic digested sludge. Water Science and Technology 63, 129-135.

Di, G., Zhu, Z., Huang, Q., Zhang, H., Zhu, J., Qiu, Y., Yin, D., Zhao, J., 2019. Targeted modulation of g-C_3N_4 photocatalytic performance for pharmaceutical pollutants in water using ZnFe-LDH derived mixed metal oxides: Structure-activity and mechanism. Science of The Total Environment 650, 1112-1121.

Dou, M., Wang, J., Gao, B., Xu, C., Yang, F., 2020. Photocatalytic difference of amoxicillin and cefotaxime under visible light by mesoporous g-C_3N_4: mechanism, degradation pathway and DFT calculation. Chemical Engineering Journal 383, 123134.

Durrani, W.Z., Nasrullah, A., Khan, A.S., Fagieh, T.M., Bakhsh, E.M., Akhtar, K., Khan, S.B., Din, I.U., Khan, M.A., Bokhari, A., 2022. Adsorption efficiency of date palm based activated carbon-alginate membrane for methylene blue. Chemosphere 302, 134793.

Fedorov, K., Dinesh, K., Sun, X., Darvishi Cheshmeh Soltani, R., Wang, Z., Sonawane, S., Boczkaj, G., 2022. Synergistic effects of hybrid advanced oxidation processes (AOPs) based on hydrodynamic cavitation phenomenon – A review. Chemical Engineering Journal 432, 134191.

Fedorov, K., Plata-Gryl, M., Khan, J.A., Boczkaj, G., 2020. Ultrasound-assisted heterogeneous activation of persulfate and peroxymonosulfate by asphaltenes for the degradation of BTEX in water. Journal of Hazardous Materials 397, 122804.

Fedorov, K., Sun, X., Boczkaj, G., 2021. Combination of hydrodynamic cavitation and SR-AOPs for simultaneous degradation of BTEX in water. Chemical Engineering Journal 417, 128081.

Feng, Y., Liao, C., Kong, L., Wu, D., Liu, Y., Lee, P.-H., Shih, K., 2018. Facile synthesis of highly reactive and stable Fe-doped g-C_3N_4 composites for peroxymonosulfate activation: A novel nonradical oxidation process. Journal of Hazardous Materials 354, 63-71.

Fernandes, A., Makoś, P., Wang, Z., Boczkaj, G., 2020. Synergistic effect of TiO_2 photocatalytic advanced oxidation processes in the treatment of refinery effluents. Chemical Engineering Journal 391, 123488.

Gągol, M., Soltani, R.D.C., Przyjazny, A., Boczkaj, G., 2019. Effective degradation of sulfide ions and organic sulfides in cavitation-based advanced oxidation processes (AOPs). Ultrasonics Sonochemistry 58, 104610.

Gao, Y., Li, Y., Zhang, L., Huang, H., Hu, J., Shah, S.M., Su, X., 2012. Adsorption and removal of tetracycline antibiotics from aqueous solution by graphene oxide. Journal of Colloid and Interface Science 368, 540-546.

Gholami, P., Khataee, A., Vahid, B., Karimi, A., Golizadeh, M., Ritala, M., 2020. Sonophotocatalytic degradation of sulfadiazine by integration of microfibrillated carboxymethyl cellulose with Zn-Cu-Mg mixed metal hydroxide/g-C_3N_4 composite. Separation and Purification Technology 245, 116866.

Guo, T., Jiang, L., Huang, H., Li, Y., Wu, X., Zhang, G., 2021. Enhanced degradation of tetracycline in water over Cu-doped hematite nanoplates by peroxymonosulfate activation under visible light irradiation. Journal of Hazardous Materials 416, 125838.

He, S., Yin, R., Lai, T., Zhao, Y., Guo, W., Zhu, M., 2021a. Structure–dependent degradation of nitroimidazoles by cobalt–manganese layered double hydroxide catalyzed peroxymonosulfate process. Chemosphere 266, 129006.

He, Y., Ma, Z., Junior, L.B., 2020. Distinctive binary g-C_3N_4/MoS_2 heterojunctions with highly efficient ultrasonic catalytic degradation for levofloxacin and methylene blue. Ceramics International 46, 12364-12372.

He, Y., Zhou, S., Wang, Y., Jiang, G., Jiao, F., 2021b. Fabrication of g-C_3N_4@NiFe-LDH heterostructured nanocomposites for highly efficient photocatalytic removal of rhodamine B. Journal of Materials Science: Materials in Electronics 32, 21880-21896.

Hong, Y., Zhou, H., Xiong, Z., Liu, Y., Yao, G., Lai, B., 2020. Heterogeneous activation of peroxymonosulfate by CoMgFe-LDO for degradation of carbamazepine: Efficiency, mechanism and degradation pathways. Chemical Engineering Journal 391, 123604.

Jin, C., Wang, M., Li, Z., Kang, J., Zhao, Y., Han, J., Wu, Z., 2020. Two dimensional Co_3O_4/g-C_3N_4 Z-scheme heterojunction: Mechanism insight into enhanced peroxymonosulfate-mediated visible light photocatalytic performance. Chemical Engineering Journal 398, 125569.

Jo, W.-K., Tonda, S., 2019. Novel CoAl-LDH/g-C_3N_4/RGO ternary heterojunction with notable 2D/2D/2D configuration for highly efficient visible-light-induced photocatalytic elimination of dye and antibiotic pollutants. Journal of Hazardous Materials 368, 778-787.

549 Karim, A.V., Shriwastav, A., 2021. Degradation of amoxicillin with sono, photo, and
550 sonophotocatalytic oxidation under low-frequency ultrasound and visible light. Environmental
551 Research 200, 111515.
552 Kim, J.R., Kan, E., 2016. Heterogeneous photocatalytic degradation of sulfamethoxazole in
553 water using a biochar-supported TiO_2 photocatalyst. Journal of Environmental Management 180,
554 94-101.
555 Lestari, P.R., Takei, T., Kumada, N., 2021. Novel ZnTi/C_3N_4/Ag LDH heterojunction composite
556 for efficient photocatalytic phenol degradation. Journal of Solid State Chemistry 294, 121858.
557 Li, S., Yang, Y., Zheng, H., Zheng, Y., Jing, T., Ma, J., Nan, J., Leong, Y.K., Chang, J.-S., 2022.
558 Advanced oxidation process based on hydroxyl and sulfate radicals to degrade refractory organic
559 pollutants in landfill leachate. Chemosphere 297, 134214.
560 Liu, W.-J., Dang, L., Xu, Z., Yu, H.-Q., Jin, S., Huber, G.W., 2018. Electrochemical oxidation of
561 5-hydroxymethylfurfural with NiFe layered double hydroxide (LDH) nanosheet catalysts. ACS
562 Catalysis 8, 5533-5541.
563 Motlagh, P.Y., Khataee, A., Hassani, A., Rad, T.S., 2020. ZnFe-LDH/GO nanocomposite coated
564 on the glass support as a highly efficient catalyst for visible light photodegradation of an
565 emerging pollutant. Journal of Molecular Liquids 302, 112532.
566 Naderi, M., Darvishi Cheshmeh Soltani, R., 2021. Hybrid of ZnFe layered double
567 hydroxide/nano-scale carbon for activation of peroxymonosulfate to decompose ibuprofen:
568 Thermodynamic and reaction pathways investigation. Environmental Technology & Innovation
569 24, 101951.
570 Qin, Y., Wang, L., Wang, X., 2019. A high performance sensor based on PANI/ZnTi-LDHs
571 nanocomposite for trace NH_3 detection. Organic Electronics 66, 102-109.

572 Rad, T.S., Khataee, A., Arefi-Oskoui, S., Rad, S.S., Orooji, Y., Gengec, E., Kobya, M., 2022.
573 Graphene-based ZnCr layered double hydroxide nanocomposites as bactericidal agents with high
574 sonophotocatalytic performances for degradation of rifampicin. Chemosphere 286, 131740.
575 Ramachandran, R., Thangavel, S., Minzhang, L., Haiquan, S., Zong-Xiang, X., Wang, F., 2021.
576 Efficient degradation of organic dye using Ni-MOF derived NiCo-LDH as peroxymonosulfate
577 activator. Chemosphere 271, 128509.
578 Shahzad, A., Ali, J., Ifthikar, J., Aregay, G.G., Zhu, J., Chen, Z., Chen, Z., 2020. Non-radical
579 PMS activation by the nanohybrid material with periodic confinement of reduced graphene oxide
580 (rGO) and Cu hydroxides. Journal of Hazardous Materials 392, 122316.
581 Sharma, V., Kumar, R.V., Pakshirajan, K., Pugazhenthi, G., 2017. Integrated adsorption-
582 membrane filtration process for antibiotic removal from aqueous solution. Powder technology
583 321, 259-269.
584 Soltani, R.D.C., Jafari, A.J., Khorramabadi, G.S., 2009. Investigation of cadmium (II) ions
585 biosorption onto pretreated dried activated sludge. American Journal of Environmental Sciences
586 5, 41.
587 Soltani, R.D.C., Khataee, A.R., Godini, H., Safari, M., Ghanadzadeh, M.J., Rajaei, M.S., 2015.
588 Response surface methodological evaluation of the adsorption of textile dye onto
589 biosilica/alginate nanobiocomposite: thermodynamic, kinetic, and isotherm studies. Desalination
590 and Water Treatment 56, 1389-1402.
591 Soltani, R.D.C., Mahmoudi, M., Boczkaj, G., Khataee, A., 2020. Activation of
592 peroxymonosulfate using carbon black nano-spheres/calcium alginate hydrogel matrix for
593 degradation of acetaminophen: Fe_3O_4 co-immobilization and microbial community response.
594 Journal of Industrial and Engineering Chemistry 91, 240-251.

595 Soltani, R.D.C., Mashayekhi, M., Jorfi, S., Khataee, A., Ghanadzadeh, M.-J., Sillanpää, M.,
596 2018. Implementation of martite nanoparticles prepared through planetary ball milling as a
597 heterogeneous activator of oxone for degradation of tetracycline antibiotic: ultrasound and
598 peroxy-enhancement. Chemosphere 210, 699-708.
599 Soltani, R.D.C., Miraftabi, Z., Mahmoudi, M., Jorfi, S., Boczkaj, G., Khataee, A., 2019. Stone
600 cutting industry waste-supported zinc oxide nanostructures for ultrasonic assisted decomposition
601 of an anti-inflammatory non-steroidal pharmaceutical compound. Ultrasonics Sonochemistry 58,
602 104669.
603 Song, B., Zeng, Z., Zeng, G., Gong, J., Xiao, R., Ye, S., Chen, M., Lai, C., Xu, P., Tang, X.,
604 2019. Powerful combination of g-C_3N_4 and LDHs for enhanced photocatalytic performance: a
605 review of strategy, synthesis, and applications. Advances in Colloid and Interface Science 272,
606 101999.
607 Wang, H., Mustafa, M., Yu, G., Östman, M., Cheng, Y., Wang, Y., Tysklind, M., 2019.
608 Oxidation of emerging biocides and antibiotics in wastewater by ozonation and the electro-
609 peroxone process. Chemosphere 235, 575-585.
610 Wang, Y., Zhou, S., Zhao, G., Li, C., Liu, L., Jiao, F., 2020. Fabrication of $SnWO_4$/ZnFe-layered
611 double hydroxide composites with enhanced photocatalytic degradation of methyl orange.
612 Journal of Materials Science: Materials in Electronics 31, 12269-12281.
613 Wu, J., Zhang, H., Oturan, N., Wang, Y., Chen, L., Oturan, M.A., 2012. Application of response
614 surface methodology to the removal of the antibiotic tetracycline by electrochemical process
615 using carbon-felt cathode and DSA (Ti/RuO_2–IrO_2) anode. Chemosphere 87, 614-620.

Xie, M., Tang, J., Kong, L., Lu, W., Natarajan, V., Zhu, F., Zhan, J., 2019. Cobalt doped g-C_3N_4 activation of peroxymonosulfate for monochlorophenols degradation. Chemical Engineering Journal 360, 1213-1222.

Yang, H., Zhou, J., Yang, E., Li, H., Wu, S., Yang, W., Wang, H., 2021. Magnetic Fe_3O_4–N-doped carbon sphere composite for tetracycline degradation by enhancing catalytic activity for peroxymonosulfate: A dominant non-radical mechanism. Chemosphere 263, 128011.

Yin, R., Guo, W., Wang, H., Du, J., Zhou, X., Wu, Q., Zheng, H., Chang, J., Ren, N., 2018. Enhanced peroxymonosulfate activation for sulfamethazine degradation by ultrasound irradiation: performances and mechanisms. Chemical Engineering Journal 335, 145-153.

Yu, Y., Chen, D., Xu, W., Fang, J., Sun, J., Liu, Z., Chen, Y., Liang, Y., Fang, Z., 2021. Synergistic adsorption-photocatalytic degradation of different antibiotics in seawater by a porous g-C_3N_4/calcined-LDH and its application in synthetic mariculture wastewater. Journal of Hazardous Materials 416, 126183.

Zeng, H., Zhang, H., Deng, L., Shi, Z., 2020. Peroxymonosulfate-assisted photocatalytic degradation of sulfadiazine using self-assembled multi-layered CoAl-LDH/g-C_3N_4 heterostructures: performance, mechanism and eco-toxicity evaluation. Journal of Water Process Engineering 33, 101084.

Zhao, X., Niu, C., Zhang, L., Guo, H., Wen, X., Liang, C., Zeng, G., 2018. Co-Mn layered double hydroxide as an effective heterogeneous catalyst for degradation of organic dyes by activation of peroxymonosulfate. Chemosphere 204, 11-21.

638 **Figures captions**

639 **Fig. 1**. SEM images of g-C_3N_4 (a) with EDX-Map (b), ZnFe LDH (c) with EDX-Map (d) and g-
640 C_3N_4/ZnFe LDH (e) with EDX-Map (f).

641 **Fig. 2**. XRD patterns (a) along with FT-IR spectra (b) of the g-C_3N_4/ZnFe LDH heterojunction
642 and its components.

643 **Fig. 3**. DRS results and corresponding band gap energy of g-C_3N_4 (a), ZnFe LDH (b) and g-
644 C_3N_4/ZnFe LDH (c).

645 **Fig. 4**. Degradation of TC under various treatment systems (a), together with the results of
646 kinetic study (b). Experimental conditions: [TC]: 25 µM, [Oxone]: 0.4 mM, g-C_3N_4/ZnFe LDH
647 dosage: 0.2 g/L, pH: natural (unadjusted).

648 **Fig. 5**. Effect of the presence of enhancers and scavengers (a) and kinetic results associated with
649 the presence of scavengers (b). Experimental conditions: [TC]: 25 µM, [Oxone]: 0.4 mM, g-
650 C_3N_4/ZnFe LDH dosage: 0.2 g/L, pH: natural (unadjusted), [Co-existing compounds]: 0.01 M.

651 **Fig. 6**. Effect of initial pH (a), g-C_3N_4/ZnFe LDH dosage (b), TC concentration (c) and Oxone
652 concentration (d). Experimental conditions: [TC]: 10-55 µM, [Oxone]: 0.1-0.5 mM, g-
653 C_3N_4/ZnFe LDH dosage: 0.05-0.3 g/L, pH: 4.5, 7.0 and 9.0.

654

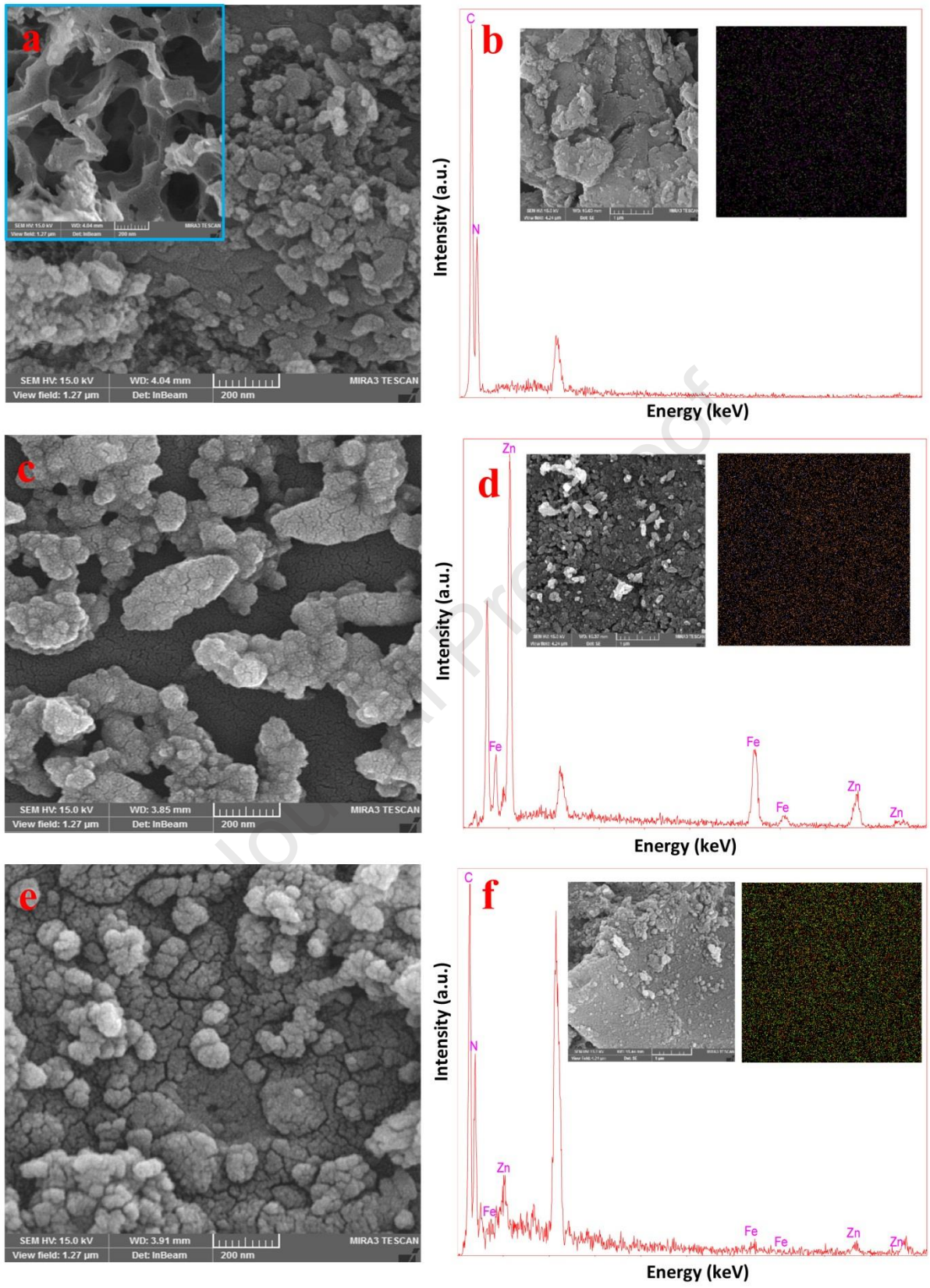

Fig. 1

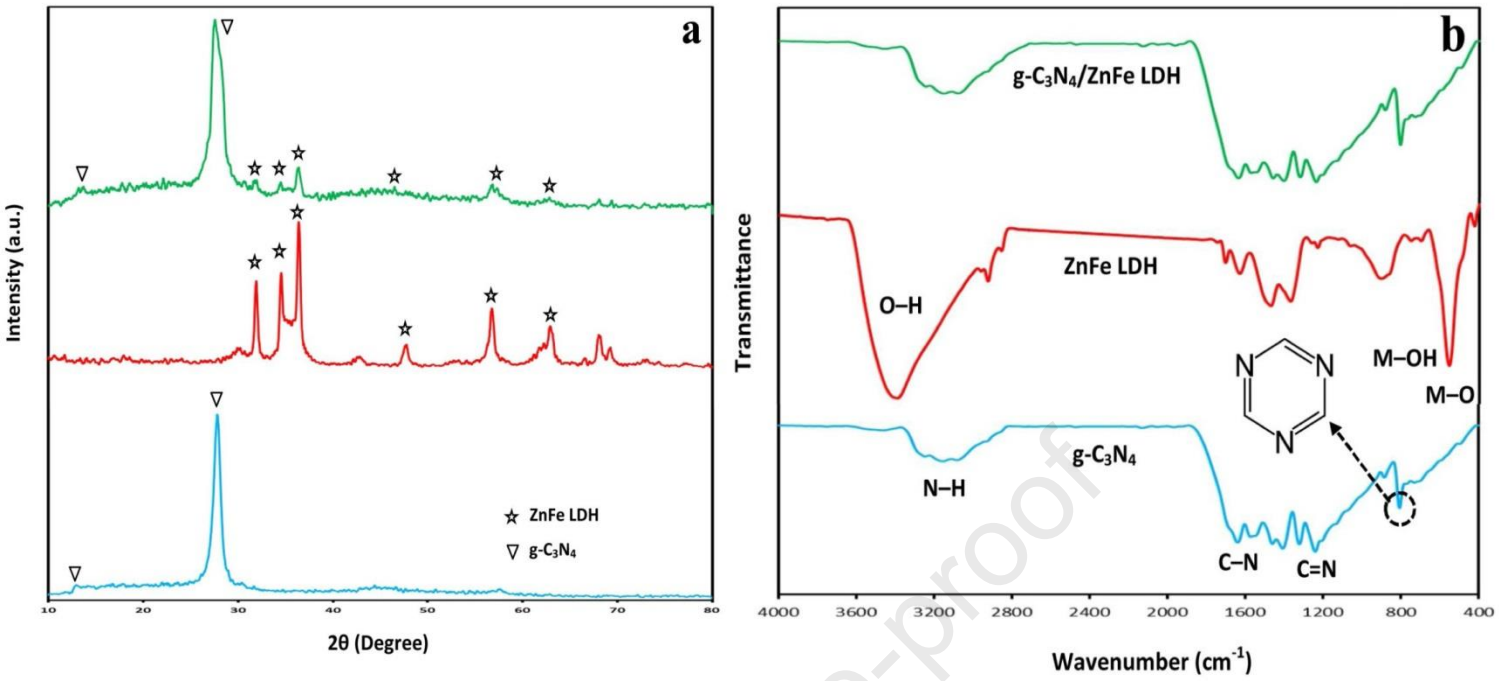

Fig. 2

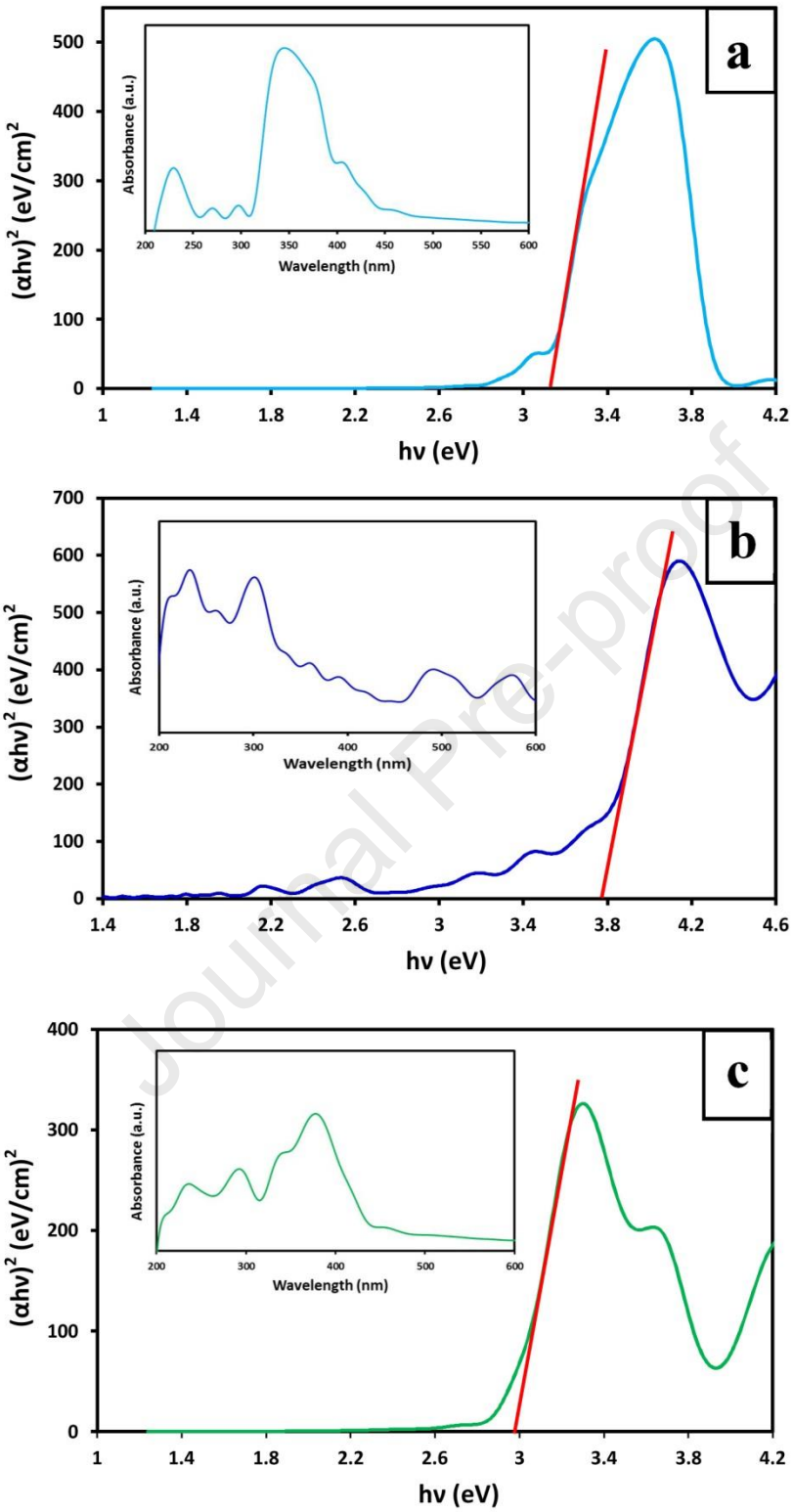

Fig. 3

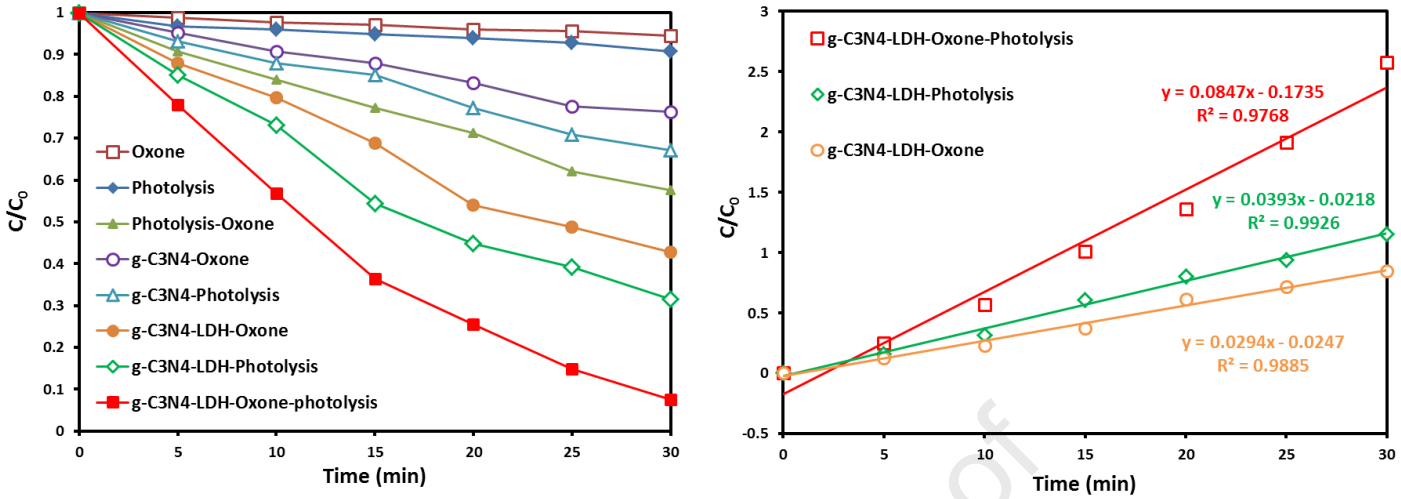

Fig. 4

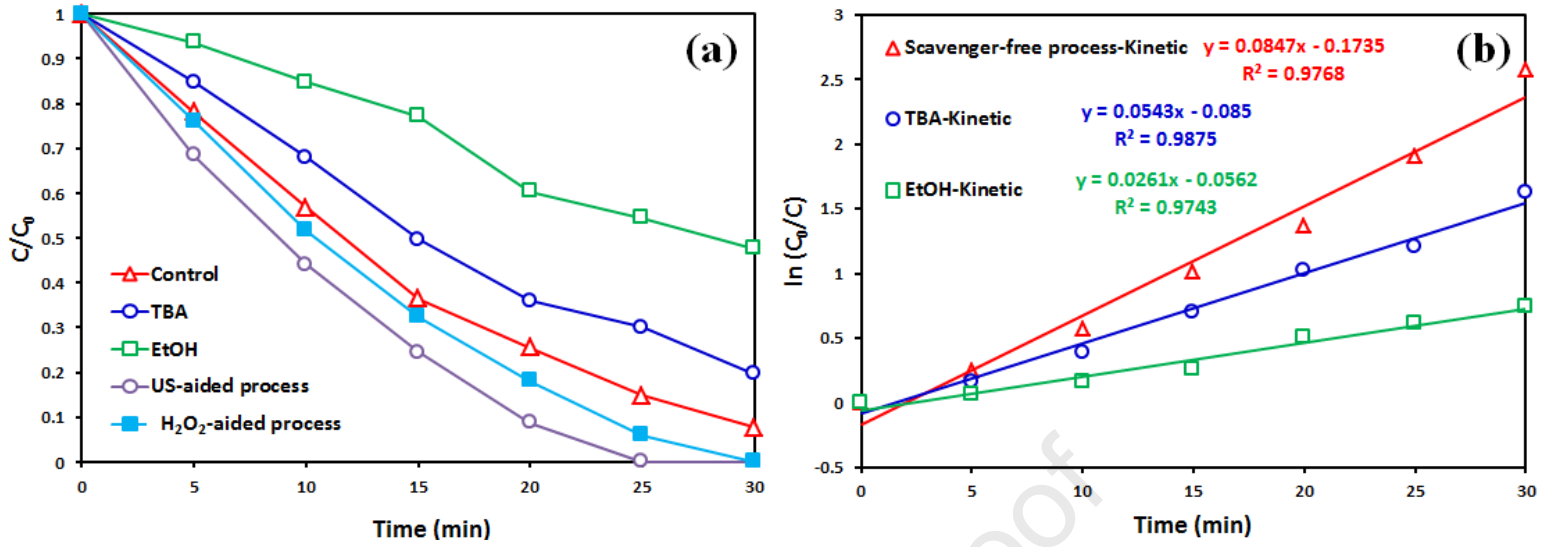

Fig. 5

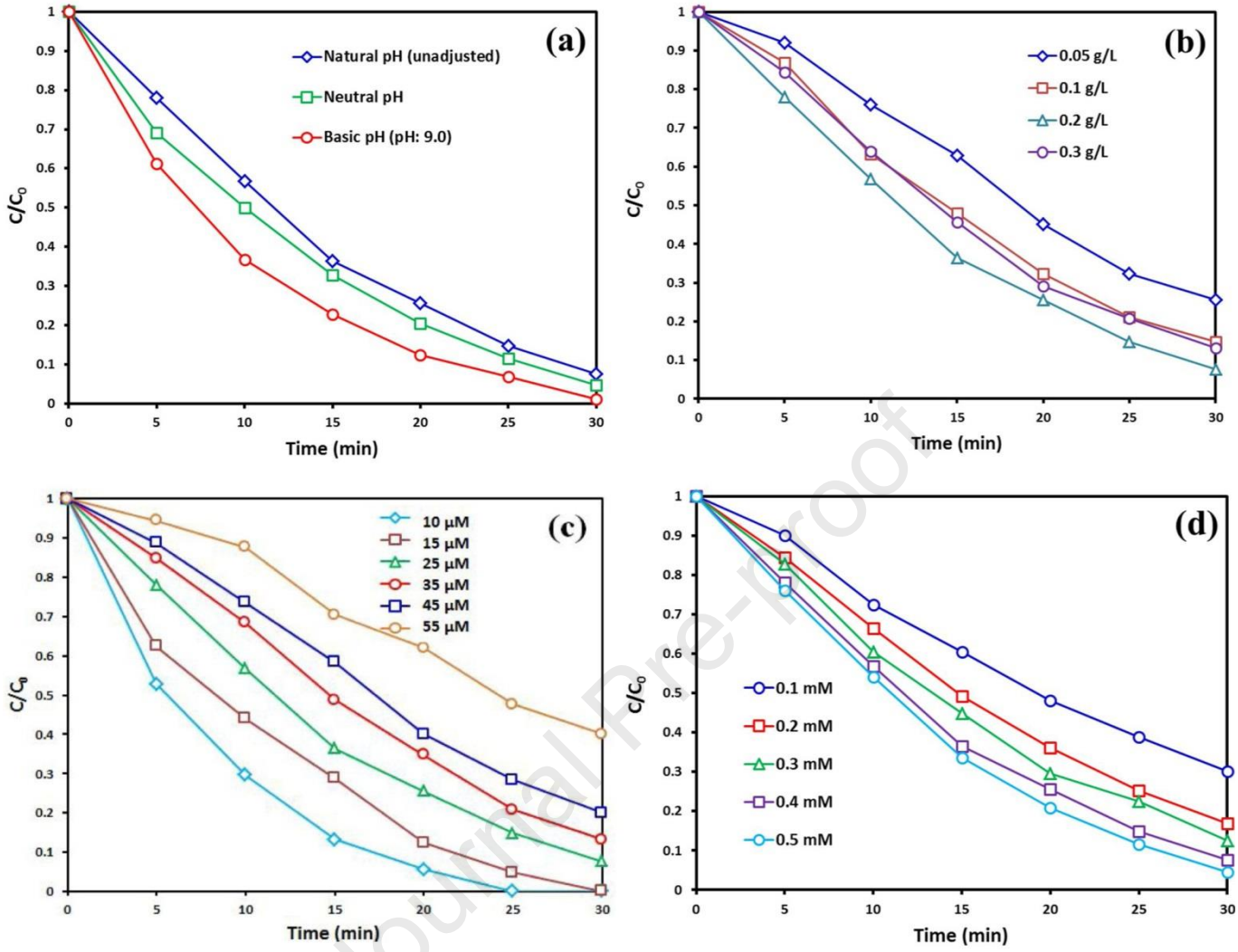

Fig. 6

Research highlights

- ✓ Binary heterojunction nanocomposite of g-C_3N_4/ZnFe LDH was synthesized as catalyst.
- ✓ Tetracycline was effectively decomposed by g-C_3N_4/ZnFe LDH/Oxone/UV process.
- ✓ Contribution of radical species to the degradation of tetracycline was determined.
- ✓ Bio-toxicity of the effluent toward microbial population was assessed.
- ✓ Enhancement of the process effectiveness was considered via ultrasound.

Declaration of competing interest

The authors declare that they have no known competing financial interests or personal relationships that could have appeared to influence the research project reported in this paper.